Meyer, Daniel ; Schumski, Lukas ; Guba, Nikolai ; Espenhahn, Björn ; Hüsemann, Tobias

Relevance of the region of interaction between the tool and the metalworking fluid for the cooling effect in grinding

Journal Article	as:	peer-reviewed accepted version (Postprint)
DOI of this document*(secondary publication):		https://doi.org/10.26092/elib/3192
Publication date of this document:		01/08/2024

* for better findability or for reliable citation

Recommended Citation (primary publication/Version of Record) incl. DOI:

D. Meyer, L. Schumski, N. Guba, B. Espenhahn, T. Hüsemann, Relevance of the region of interaction between the tool and the metalworking fluid for the cooling effect in grinding, CIRP Annals, Volume 71, Issue 1, 2022, Pages 301-304, ISSN 0007-8506, https://doi.org/10.1016/j.cirp.2022.04.055.

Relevance of the region of interaction between the tool and the metalworking fluid for the cooling effect in grinding

D. Meyer[a,c] (2)*, L. Schumski[a], N. Guba[a], B. Espenhahn[b], T. Hüsemann[a]

[a] *Leibniz Institute for Materials Engineering - IWT, Badgasteiner Str. 3, 28359 Bremen, Germany*

[b] *University of Bremen, Bremen Institute for Metrology, Automation and Quality Science (BIMAQ), Linzer Str. 13, 28359 Bremen, Germany*

[c] *MAPEX Center for Materials and Processes, University of Bremen, Postbox 330440, 28359 Bremen, Germany*

** corresponding author. Email-address: dmeyer@iwt.uni-bremen.de (D. Meyer)*

The relevance of the metalworking fluid supply characteristics is well-described for grinding processes. In the presented work, the fluid's interaction with the grinding wheel between the point of impact and the contact zone has been analyzed. For varied supply conditions, deceleration and acceleration effects are obtained and quantified. Furthermore, shadowing effects related to the fluid entrainment towards the contact zone are considered. The observed effects within the region of interaction are consistent with the thermal limits of taper grinding experiments. By revealing the fluid's behavior within the region of interaction, explanation for the effectiveness of supply conditions is given.

Keywords: Grinding, Cooling, Supply

1. Introduction and target of research

Limiting the thermal load in grinding [1] to avoid thermal damage of the workpiece material is a well-described challenge. Besides adaptations of the process parameters and the tool specifications, the choice of metalworking fluids (MWFs) [2] and their supply [3] are major factors allowing for increasing productivity and reducing the risk of grinding burn. With regard to the sufficient supply of the contact zone between the grinding wheel and the workpiece, the relevance of the nozzle design [4], the flowrate [5], and the free jet characteristics (including velocity) [6] have been determined and general interrelations were revealed. The nozzle design should lead to a coherent flow of the free jet to avoid air entrainment, the free jet's velocity should be within the range of the wheel speed or slightly lower, a certain flow rate per mm width of the grinding wheel is required, and the jet should impinge the wheel tangentially to allow beneficial MWF entrainment. Accompanying the analysis of the MWF supply, its effects have been quantified based on the thermal conditions in the contact zone [7] and with respect to the resulting surface and subsurface characteristics of the workpiece [8, 9].

A factor that was not studied in depth yet is the relevance of the interaction of the MWF with the grinding wheel starting from the free jet's point of impact P_i followed by the entrainment and transport of the MWF towards the contact zone. As the model-based and experimental analysis of this region of interaction is challenging, the gap between the knowledge concerning the free jet and the cooling effects within the contact zone remained open.

The presented work aims to reveal mechanisms of effective MWF supply by analyzing the so far unknown fluid behavior within this region of interaction. An experimental approach is chosen to gain insights regarding the velocity and distribution of the fluid within the region of interaction for varied supply parameters. Based on time resolved high-speed video images, shadowgraphy analysis and shadowgram image velocimetry (SIV) [10] were performed and correlated with cooling effects and the thermal limits in taper grinding. Figure 1 summarizes the general approach specifically aiming at quantifying the observed effects and deducing explanation for the effectiveness of the MWF supply in grinding.

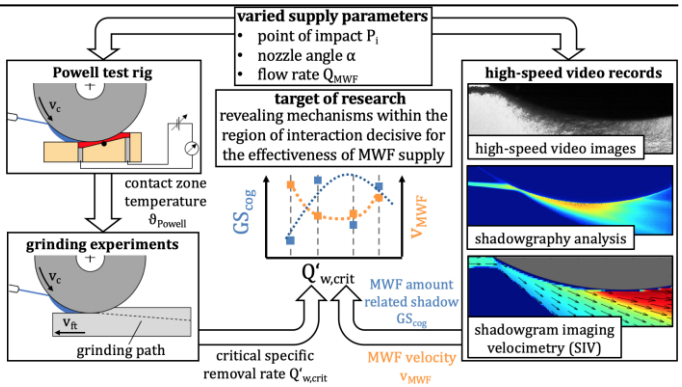

Figure 1. Approach to reveal the relevance of the region of interaction for the effectiveness of MWF supply in grinding.

2. Experimental setup and analysis

An oil-based MWF was supplied by a free jet nozzle with a Rouse [11] inner profile and an outlet cross-section A of 25 mm² (height x width = 1.25 mm x 20 mm). By varying the free jet's point of impact P_i ($P_i(r_0;\phi)$, with r_0 being the radius of the grinding wheel and ϕ being the angle in the polar coordinate system) on the grinding wheel, the nozzle angle α, the velocity ratio v ($v = v_{jet}/v_c$), and the flow rate Q_{MWF}, the decisive MWF supply parameters are considered. To reveal the mechanisms that lead to optimal supply of the contact zone and to learn what effects occur when MWF-supply deviates from the supposedly optimal conditions, the region of interaction was investigated for a wide range of favorable and unfavorable combinations of impact points and nozzle angles.

The influence of the varied supply conditions was determined in a) a test rig based on Powell [12] to analyze the cooling effect, b) high-speed video records to gain data for the analysis of the velocity (SIV) and the entrainment (shadowgraphy analysis) of the MWF in the region of interaction, and c) taper face grinding experiments revealing the critical specific material removal rate $Q'_{w,crit}$ defined here by the onset of a heat-affected zone within the workpiece. The setup is summarized in Fig. 2 indicating the varied parameters and their values.

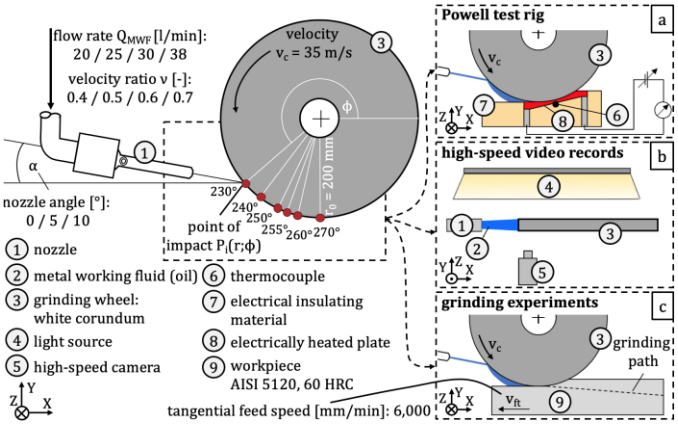

Figure 2. Experimental setup and varied parameters.

2.1. Analysis of the cooling effect for varied MWF supply conditions

To evaluate the temperature in the contact zone between the grinding wheel and the workpiece for different MWF supply conditions, the test rig shown in Fig. 2a was developed based on the investigations of Powell [12]. The grinding wheel is fed into an electrically heated plate until the contact zone is completely formed. The feed motion is then stopped (v_{ft} = 0 mm/min), and the grinding wheel's circumferential velocity v_c = 35 m/s is maintained. With a constant heating power, the temperature change due to varying MWF supply conditions was determined using a thermocouple located under the grinding arc in the center of the contact zone. The temperatures in the Powell test rig are generally lower than those in grinding processes. However, the reliability of this test rig for the analysis of the cooling effect has been demonstrated in previous studies [13, 14, 15].

2.2. Identification of the thermal limits in taper face grinding

The grinding experiments were performed on the surface grinder Elb MicroCut A8 using a white corundum grinding wheel A80G12V09C (diameter x width = 400 mm x 20 mm). Workpieces (height x width x depth = 30 mm x 80 mm x 20 mm) made of AISI 5120 (60 HRC) were used. So-called taper grinding tests (taper angle: 0.16°) were carried out. During these, the depth of cut a_e was continuously increased from 0 µm to 180 µm at a constant tangential feed speed v_{ft} = 6,000 mm/min (see Fig. 2c). In taper grinding, a wide range of specific material removal rates Q'_w and thus thermal loads can be realized. To identify potential outliers, each test was performed three times. The workpieces were pre-ground (a_e = 50 µm; v_{ft} = 500 mm/min). Before each experiment, the grinding wheel was dressed with a single point dresser (a_{ed} = 3 x 30 µm; overlapping ratio U_d = 3).

As exemplarily shown in Fig. 3, grinding forces have been measured using a Kistler dynamometer (type 9255B) and metallographic cross-sections in the grinding direction were prepared for the identification of thermal damage. The onset of tempering zones (dark areas in Fig. 3) was defined as the beginning of thermal damage. Furthermore, residual stresses at the ground surfaces were measured in the cutting speed direction by X-ray diffraction to confirm the thermal effects determined with the metallographic cross-sections. As exemplarily shown in Fig. 3, the increasing thermal load in taper grinding is accompanied by a transition from compressive to tensile residual stresses shortly before and at the beginning of the tempering zone. Here, the critical specific material removal rate $Q'_{w.crit}$ as well as the tangential and the normal force $F_{t,crit}$ and $F_{n,crit}$ were determined.

2.3. Analysis of the fluid's behavior in the region of interaction

The challenging task to get deeper insights into the fluid-tool-interaction within the region of interaction was approached by two evaluation methods for high-speed video records. In both cases, the analysis was performed with a rotating grinding wheel but without a workpiece in place to ensure good optical accessibility.

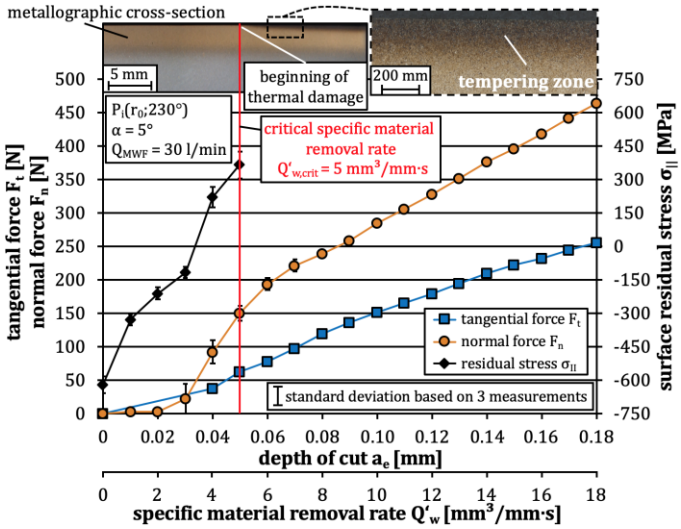

Figure 3. Exemplary determination of the critical specific material removal rate for $P_i(r_0;230°)$ α = 5° and Q_{MWF} = 30 l/min.

The shadowgraphy analysis targets the entrainment and distribution of MWF in the area between the point of impact and the contact zone. As shown in Fig. 2b, the MWF flow was recorded using a high-speed camera positioned orthogonally to the grinding wheel. The MWF and the grinding wheel were located between a diffuse light source (LED panel with 2400 lm, neutral white) and the high-speed camera (type Pro Y4 from Co. Design Tools Motion, 105 mm F2,8 EX macro objective from Co. Sigma), which were aligned collinearly to each other. The uniform background illumination resulted in a shadow cast, which in turn was captured by the camera. The intensity of the shadow is affected by the number of interfaces passed by the light and the amount of MWF in the evaluated area. As this technique is applied to highly turbulent two-phase systems for the first time, established models allowing for discriminating the effects are lacking. However, it is assumed that in the investigations, the fluid quantity correlates with the shadowing effects. For a reliable evaluation, each 1,000 8-bit greyscale images were recorded at a frame rate of 10,000 frames per second for the investigated MWF supply conditions. A reference image showing the setup without MWF supply was subtracted from all images at the beginning. As a result, only the greyscale values of the shadows caused by the MWF remained in the analyzed images. Then, a mean value image was generated from the 1,000 images to neglect random effects within the MWF flow. The resulting greyscale values are presented as a false color image for a better visualization (c.f. Fig. 5, top). The relevant zone for supplying the contact zone in grinding experiments was defined to be located between the lowest point of the grinding wheel and 15 mm towards the MWF nozzle and has a pixel-related height of 5.4 mm. The greyscale values within this zone have been evaluated in the form of histograms. For a quantitative comparison of the shadowing effects in the relevant zone, the position of the center of gravity (*cog*) of the histograms on the axis representing the greyscale (*GS*) values has been deduced (Fig. 5, bottom).

To evaluate the MWF's velocity v_{MWF} within the region of interaction, shadowgram imaging velocimetry (SIV) was applied. A cross-correlation algorithm [10] uses striking structures within the observed flow and tracks their position across the recorded images. The corresponding velocity can be calculated from the distance covered by the individual structures and the time elapsed, which results from the frame rate of the camera with a spatial resolution of 1.82 x 1.82 mm². The accumulation of the individual velocities results in a time-averaged velocity field. Velocities were quantified for the relevant zone of interaction starting at the point of impact P_i and ending at the lowest point of the grinding wheel (Fig. 6). Thus, the analyzed distance varies based on the chosen P_i.

3. Results

3.1 Cooling effect and critical specific material removal rate

The Powell test rig was used to quantify the temperature ϑ_{Powell} in the contact zone for the various supply conditions. The lowest temperatures were found at a point of impact $P_i(r_0;255°)$ and a nozzle angle α = 5° (Fig. 4). Compared to $P_i(r_0;255°)$, a significant temperature increase is observed especially at points with lower ϕ -values.

Since the Powell test rig does not represent real grinding conditions, grinding experiments were performed to quantify the effects of the varying cooling performance of the varied supply conditions. According to the criteria shown in Fig. 3, the critical specific material removal rates and the force ratio at this point μ_{crit} were determined after the grinding experiments and are also shown in Fig. 4. Depending on the supply conditions, the critical specific material removal rate varies from 4.8 mm³/mm·s to 11.4 mm³/mm·s reconfirming the significant relevance of the MWF supply.

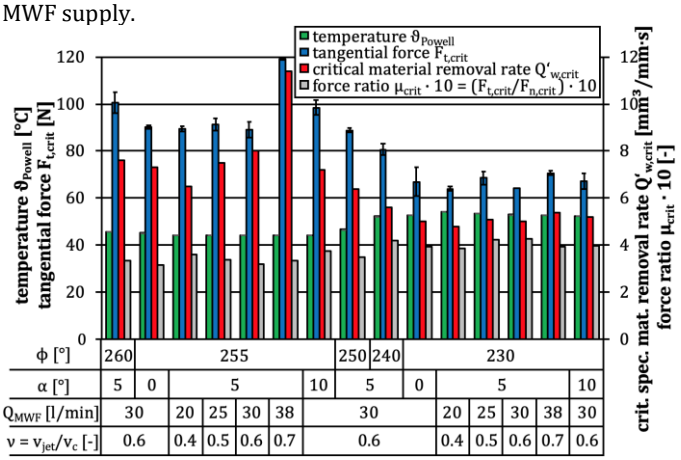

Figure 4. Influence of the MWF supply conditions on the temperature, the tangential force, the force ratio and the critical specific material removal rate.

For a point of impact of $P_i(r_0;255°)$ and a nozzle angle α of 5°, $Q'_{w,crit}$ increases from 6.5 mm³/mm·s to 11.4 mm³/mm·s with higher flow rates Q_{MWF}. A constant flow rate of Q_{MWF} = 30 l/min at a nozzle angle of α = 5° leads to critical specific material removal rates of $Q'_{w,crit}$ = 5.0 mm³/mm·s ($P_i(r_0;230°)$) to 8.0 mm³/mm·s ($P_i(r_0;255°)$). For a point of impact of $P_i(r_0;230°)$, even a higher flow rate does not lead to a relevant increase in the achievable critical specific material removal rate. The insufficient MWF supply at points of impact with $\phi < 255°$ is reflected in the reduced cooling effect (ϑ_{Powell} is approx. 20 % higher compared to similar supply conditions at $P_i(r_0;255°)$) but also in the increasing friction within the contact zone resulting in higher force ratios μ_{crit}. The combination of insufficient cooling and lubrication consequently leads to the lower critical specific material removal rates in the grinding experiments. As already determined with the help of the Powell test rig, it can be confirmed by the grinding experiments that the optimal MWF supply of the contact zone is obtained at an impact point of $P_i(r_0;255°)$ and a nozzle angle of α = 5°. Under these supply conditions, additional cooling effects can only be achieved at increased MWF flow rates.

These findings agree with the current state of knowledge. According to e.g. [4, 16, 17], the vertical distance to the contact zone (here the impact point) should be as short as possible and the nozzle angle should not exceed a value of α = 20°. In the present study, points of impact with ϕ > 255° and thus an even shorter vertical distance to the contact zone do not result in an improvement of the cooling effect. Instead, an increase of the temperature ϑ_{Powell} and a decrease of the critical specific material removal rate is found for $P_i(r_0;260°)$.

3.2 MWF entrainment and distribution towards the contact zone

Depending on the MWF supply conditions, varying amounts of MWF are transported towards the contact zone based on the interaction of the fluid and the grinding wheel's surface. Quantitative analysis of the shadowing effects within the relevant area was achieved as described in section 2.3. Figure 5 exemplarily shows the time-averaged grey values of 1,000 images in false color for a point of impact of $P_i(r_0;255°)$, a nozzle angle α = 5°, and a flow rate of Q_{MWF} = 30 l/min. For a constant nozzle angle of α = 5° and a constant flow rate of Q_{MWF} = 30 l/min, the shadowing effect caused by the MWF within this evaluation area is quantified by means of histograms of the greyscale values *GS* (Fig. 5, bottom). The high frequency of occurrence n_i of high greyscale values for $P_i(r_0;250°)$ and $P_i(r_0;255°)$ indicates intense shadowing effects assumed to be significantly caused by superior supply of this area with MWF. The histograms for $P_i(r_0;240°)$ and $P_i(r_0;260°)$ are shifted to lower greyscale values. For $P_i(r_0;260°)$, the comparably low greyscale values can be traced back to a lower number of interfaces (less atomization of the jet) affecting the applied evaluation method. Poor supply of this area for $P_i(r_0;230°)$ is obvious from the images and low greyscale values are obtained for this supply condition. The abscissa position of the center of gravity (*cog*) is quantified for each histogram as exemplarily shown for $P_i(r_0;255°)$ and $P_i(r_0;260°)$. The values for GS_{cog} are used for further analysis of the observed phenomena (see Fig. 7). Here, the significantly reduced turbulence at $P_i(r_0;260°)$ affects the evaluation as reflected by the noticeably dissimilar shape of the histogram. This leads to a GS_{cog} shifted to a low value which is considered as an outlier. The supply of the relevant area can be expected to be better than indicated.

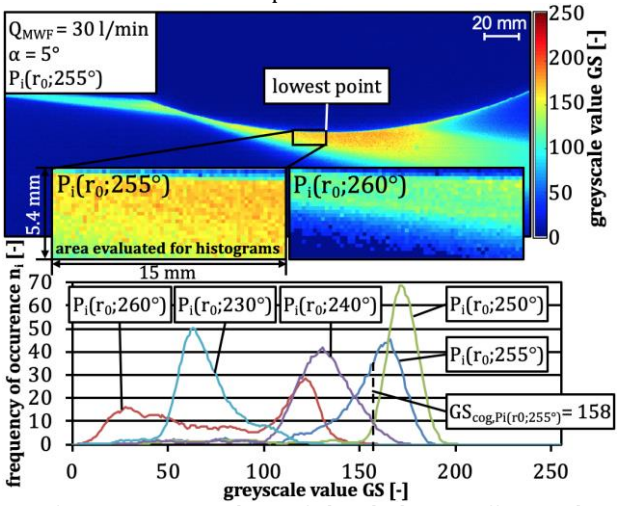

Figure 5. Quantitative analysis of the shadowing effects within the evaluation area under varied supply conditions.

3.3 Deceleration and acceleration within the region of interaction

For the MWF supply conditions analyzed in more detail (α = 5°, Q_{MWF} = 30 l/min), a velocity of the free jet of v_{jet} = 20 m/s was experimentally confirmed by SIV. In Fig. 6, a velocity field within the region of interaction is presented exemplarily for $P_i(r_0;255°)$. Quantitative analysis of the velocity (along the path starting at the point of impact towards the lowest point of the grinding wheel is given for all variations of P_i. The velocity values represent the average value over vertical lines within the area of evaluation (red lines in Fig. 6) with a length of 5.4 mm each and a horizontal distance of 1.82 mm. The SIV measurements reveal that for all supply conditions, an initial deceleration of the MWF is occurring. For $P_i(r_0;230°)$, it takes the MWF more than 20 mm within the region of interaction to be accelerated back to v_{jet} by the grinding wheel. Velocities of v_{MWF} = 26 m/s are achieved for this supply condition before the deflection of the whole MWF away from the grinding wheel and a drop of the velocity are observed. The highest relative uncertainty for v_{MWF} of 1.2% was observed for $P_i(r_0;230°)$.

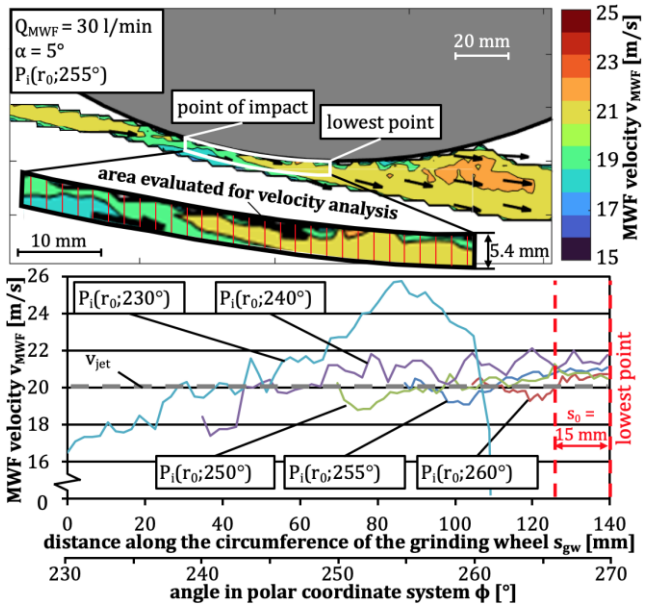

Figure 6. MWF velocity map ($P_i(r_0;255°)$) and velocity development within the region of interaction for varied supply conditions.

For ϕ > 240°, deceleration is less pronounced but also the available distance along the wheel's circumference for acceleration is shorter. For further quantitative analysis (see Fig. 7), the mean velocity over the last s_0 = 15 mm prior to the lowest point of the grinding wheel $\bar{v}_{MWF,s0}$ is deduced from the data. The influence of the so far unknown deceleration/re-acceleration effects within the region of interaction on the MWF velocity at the lowest point of the grinding wheel was revealed here for the first time.

3.4 Relevance of the observed effects for thermal limits in grinding

The presented analysis methods allow quantitative insights into the region of interaction, which have been denied so far. Interpretation of the observed effects in terms of an explanation of the mechanisms for effective cooling performance in grinding is now possible. As shown in Fig. 7, the lowest critical specific material removal rate is achieved at low values for GS_{cog}. Even at very high velocities of the MWF. This suggests that in a certain range (blue double arrow) of the analyzed variables, the achievable $Q'_{w,crit}$ is dominated by the effects leading to shadowing effects. When a certain level of MWF entrainment prevails, small increases of the MWF's velocity are observed for higher $Q'_{w,crit}$. When sufficient supply of the contact zone is provided, the influence of $\bar{v}_{MWF,s0}$ appears to be dominant (range indicated by orange double arrow). The highest value for $Q'_{w,crit}$ results from a situation characterized by GS_{cog} and $Q'_{w,crit}$ being at a decent level. The dotted lines in Fig. 7 represent assumed progressions whose course can now be uncovered for various grinding operations based on the presented approach.

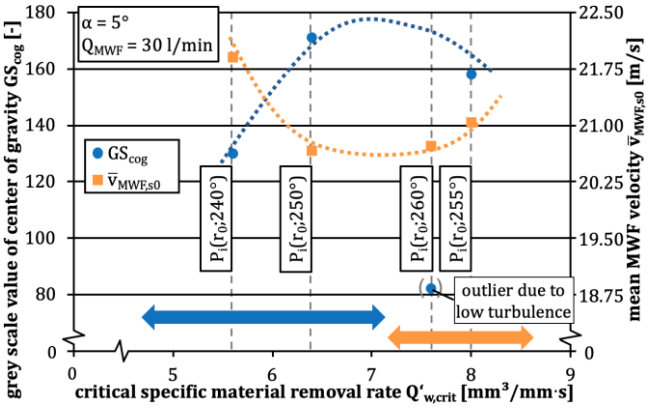

Figure 7. Critical specific material removal rates correlated with the observed parameters within the region of interaction.

4. Conclusions

In the presented taper grinding experiments, the variation of the MWF supply conditions was found to significantly affect the achievable critical specific material removal rate (up to factors > 2). The applied SIV for the first time revealed deceleration (5-15% velocity drop) and re-acceleration effects on the MWF's path from the point of impact towards the contact zone. Depending on the position of the point of impact, the distance for re-acceleration may not be sufficient to achieve the velocity ratios to be required according to literature. The yet unknown deceleration effects explain why under certain supply conditions, a high initial velocity of the free jet is crucial.

For turbulent conditions and pronounced atomization of the jet in the region of interaction, the shadowing effects quantified in the relevant zone by shadowgraphy analysis are in line with the thermal limits resulting from the taper grinding experiments. The results suggest that there is a certain minimum value of GS_{cog} essential for high $Q'_{w,crit}$ values. Under turbulent conditions, the highest critical specific material removal rates are achieved when GS_{cog} and $\bar{v}_{MWF,s0}$ both are at certain required levels. This leads to a plausible overall explanation of the phenomena described in literature: MWF supply is effective when deceleration effects are avoided or (over-)compensated by re-acceleration and a sufficient amount of MWF is transported towards the contact zone. This mechanism of effective MWF supply in grinding was exposed by the presented approach analyzing the fluid's behavior within the region of interaction between the MWF and the grinding wheel.

Acknowledgements

The presented work has gratefully been funded by the Deutsche Forschungsgemeinschaft (DFG, German Research Foundation) - ME 4447/5-1, FI 1989/4-1, project Nr. 415003387. The authors express their deep gratitude to Prof. A. Fischer and Dr. D. Stöbener (BIMAQ) for the profound discussions within this collaboration.

References

[1] Malkin, S., Guo, C., 2007, Thermal Analysis in Grinding, Annals of the CIRP, 56/2: 760-782.

[2] Brinksmeier, E., Meyer, D., Huesmann-Cordes, A.G., Herrmann, C., 2015, Metalworking Fluids – Mechanisms and Performance, Annals of the CIRP, 64/2: 605-628.

[3] Heinzel, C., Kirsch, B., Meyer, D., Webster, J., 2020, Interactions of grinding tool and supplied fluid, Annals of the CIRP, 69/2: 624-645.

[4] Webster, J.A., Cui, C., Mindek, R.B., 1995, Grinding fluid application system design. Annals of the CIRP, 44/1: 333-338.

[5] Webster, J.A., 2008, In grinding coolant application matters, Manufacturing engineering, 140/3.

[6] Brinksmeier, E., Heinzel, C., Wittmann, M., 1999, Friction, Cooling and Lubrication in Grinding, Annals of the CIRP, 48/2: 581-598.

[7} Brinksmeier, E., Aurich, J.C., Govekar, E., Heinzel, C., Hoffmeister, H.W., Klocke, F., Peters, J., Rentsch, R., Stephenson, D.J., Uhlmann, E., Weinert, K., Wittmann, M., 2006, Advances in Modeling and Simulation of Grinding Processes, Annals of the CIRP, 55/2: 667-696.

[8] Meyer, D., Wagner, A., 2016, Influence of metalworking fluid additives on the thermal conditions in grinding, Annals of the CIRP, 65/1: 313-316.

[9] Jamshidi, H., Budak, E., 2021, On the prediction of surface burn and its thickness in grinding processes, Annals of the CIRP, 70/1: 285-288.

[10] Espenhahn, B., Schumski, L., Vanselow, C., Stöbener, D., Meyer, D., Fischer, A., 2021, Feasibility of Optical Flow Field Measurements of the Coolant in a Grinding Machine. Applied Sciences, 11/11615: 1-18.

[11] Rouse, H., 1951, Experimental investigation of fire monitors and nozzles. Ed. ASCE

[12] Powell, J., 1979, The Application of Grinding Fluid in Creep Feed Grinding, Ph.D. thesis, University of Bristol.

[13] Wittmann, M., Heinzel C., Brinksmeier E., 2004, Evaluating the Efficiency of Coolant Supply Systems in Grinding, Production Engineering Research and Development, 6/2: 39-42.

[14] Howes, T.D., Neailey, K., Harrison, J., 1990, Fluid Film Boiling in Shallow Cut Grinding. Annals of the CIRP, 39/1:313-316.

[15] Heinzel, C., Meyer, D., Kolkwitz, B., Eckebrecht, J., 2015, Advanced approach for a demand-oriented fluid supply in grinding. Annals of the CIRP, 64/1: 333–336.

[16] Engineer, F., Guo, C., Malkin, S., 1992, Experimental measurement of fluid flow through the grinding zone, Journal of Engineering for Industry, 114: 61-66.

[17] Alberdi, R., Sanchez, J.A., Pombo, I., Ortega, N., 2011, Strategies for optimal use of fluids in grinding, International Journal of Machine Tools and Manufacture, 51: 491-499.